International Journal of Mass Spectrometry 306 (2011) 82–90

Contents lists available at ScienceDirect

International Journal of Mass Spectrometry

journal homepage: www.elsevier.com/locate/ijms

Fragmentation patterns of core ionized uracil

E. Itälä[a,b,*], D.T. Ha[a,b], K. Kooser[a,c], E. Nõmmiste[c], U. Joost[c,d], E. Kukk[a,e]

[a] Department of Physics and Astronomy, University of Turku, FIN-20014 Turku, Finland
[b] Graduate School of Materials Research, FIN-20500 Turku, Finland
[c] Institute of Physics, University of Tartu, Riia 142 EE-51014 Tartu, Estonia
[d] Estonian Nanotechnology Competence Center, Riia 142, EE-51014 Tartu, Estonia
[e] Turku University Centre for Materials and Surfaces (MatSurf), FIN-20014 Turku, Finland

ARTICLE INFO

Article history:
Received 17 January 2011
Received in revised form 8 July 2011
Accepted 8 July 2011
Available online 20 July 2011

Keywords:
PEPIPICO
Molecular fragmentation
Dissociation
Time-of-flight
Coincidence
Core ionization

ABSTRACT

Photofragmentation of the uracil molecule following carbon 1s core ionization and the subsequent Auger deacy has been investigated. The applied technique, photoelectron–photoion–photoion coincidence (PEPIPICO) spectroscopy allows simultaneous detection of momentum-correlated photoions together with the photoelectron and makes possible a detailed investigation of different fragmentation processes. In order to help the fragment identification, also uracil where one of the carbon atoms was replaced by ^{13}C was measured, with the assumption that replacement of one C atom by ^{13}C does not alter the fragmentation. An earlier investigation concerning thymine and 5-bromouracil was a strong motivation for the present study. The present results confirm the starting hypothesis for the pattern analysis, that the fragmentation process is preceded by only one starting geometry of the parent molecule, followed by a number of sequential bond cleavages and that all pyrimidine derivatives have very similar fragmentation behavior. However, the replacement of a hydrogen atom by methyl group, *i.e.*, the transition from uracil to thymine, seems to narrow the range of possible ion fragments.

© 2011 Elsevier B.V. All rights reserved.

1. Introduction

Uracil is a common naturally occurring pyrimidine derivative found in RNA, it base pairs with adenine and is replaced by thymine in DNA. Recently there has been vivid discussion about the possible formation and survival of nucleobases in interstellar medium and primitive earth like environments [1–6]. Some nucleobases have been found in meteoritic materials [7] and uracil have actually been produced in space-like conditions by radiating pyrimidine containing ice with UV-light [8]. The angle of the present study, however, is not directly astrochemical, medical nor biological, although all these aspects create a strong motivation. Here the purpose is to investigate the fragmentation behavior of the sample molecule following the carbon core ionization. This study is a follow-up to our recent study concerning thymine and 5-bromouracil and one of the goals is to see, how well does the hypothesis that the dicationic fragmentation starts as a straightforward pyrimidine ring cleavage work in the case of uracil. One of the consequences of this model is that all pyrimidine derivatives fragment very similarly. With thymine some calculations were also performed in order to see, how well some quite simple approximations describe the measured results. Because the calculation and the experimental results agreed so well, we intend to perform similar calculations with uracil [9].

There have been several different kinds of studies reported concerning uracil and its fragmentation [10–15], but to our knowledge only one study focused on doubly charged uracil and its fragmentation [16], although studies with similar molecules have been carried out [17–19]. The method applied here is photoelectron–photoion–photoion coincidence spectroscopy (PEPIPICO), which is a powerful tool when investigating the fragmentation of doubly ionized molecules into pairs of cations [20–23]. Since the method utilizes combined ion and energy resolved electron detection and the fragmentation follows the C 1s core ionization, one can also investigate the possible effects of the initial ionization site on fragmentation. To reduce the ambiguity in identifying ionic fragment pairs and their site origins in, the ^{13}C-labeled uracil at the C2 site was used – see Fig. 1.

One might argue that the measurements performed in vacuum conditions and with isolated molecules are not comparable with those in human tissue. However, the high energies involved in these reactions and the resulting rapid reaction make solvent effects negligible. That is, the same initial reactions would take place in the tissue as in the gas phase. Also, the experiments on isolated molecules provide essential and most fundamental information about the fragmentation induced by core ionization. Therefore it is imperative to truly understand the processes in single molecule

* Corresponding author at: Department of Physics and Astronomy, University of Turku, FIN-20014 Turku, Finland.
E-mail address: ersita@utu.fi (E. Itälä).

1387-3806/$ – see front matter © 2011 Elsevier B.V. All rights reserved.
doi:10.1016/j.ijms.2011.07.006

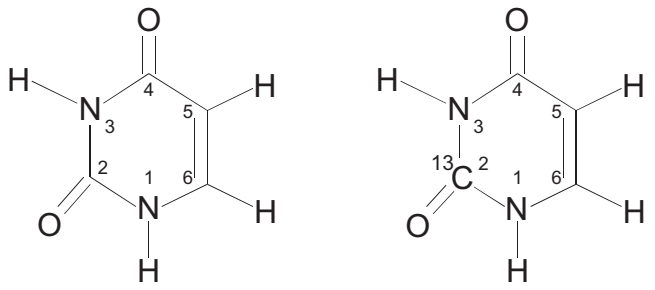

Fig. 1. Investigated sample molecules; uracil (a) and ^{13}C-uracil (b).

induced by core ionization, before the effects of chemical environment on fragmentation can begin to unveil.

2. Experimental

The apparatus and method for the present photoelectron–photoion–photoion coincidence (PEPIPICO) measurements has already been described in detail in Ref. [24], and only a brief summary is given here. The apparatus consists of a modified Scienta SES-100 electron energy analyzer [25], where the original CCD camera was replaced by a resistive anode detector (Quantar), and a home-made Wiley-Mclaren type ion time-of-flight detector with a 400 mm long drift tube. The ion spectrometer is equipped by 77 mm Hamamatsu MCP detector with the anode consisting of 10 concentric rings. The ion TOF is determined by the recharge signal pulse from the MCP stack and the pulses from the anode rings are delayed by 50–100 ns with 5 ns steps. These can be used to determine the radial hit distance from the instrument's axis. The ion detection electronics is based on a 1 GHz waveform digitizer card (Signatec PDA 1000). For the PEPIPICO measurements, the PEPICO system is operated in the pulsed extraction field mode and in the present experiment the extraction pulse voltage was 200 V across the sample region, with the drift tube held at −1100 V. The ion extraction pulses were triggered by the fast preamplifier signal from the electron detector. Uracil sample was introduced into the photoionization region by evaporation from a heated oven (MBE Komponenten NTEZ40 oven) maintained between 160 and 170 °C.

The PEPIPICO data always contain some "false" coincidences of particles not originating from the same molecule. The probability of such events was kept small by using low counting rates <20 electrons/s. In addition, artificial coincidence events were created during the measurement by a pulse generator so that two ion–ion coincidence maps were collected simultaneously – one in coincidence with electrons and one triggered by pulse generator. The average number of ions per electron trigger was 0.8 and number of ions per artificial trigger 0.2 (including detector noise counts).

The ions were measured in coincidence with the C 1s photoelectrons at $h\nu = 315$ eV and using the electron kinetic energy window with range from 17 eV to 27 eV. The pass energy of the electron spectrometer was 100 eV and the entrance slit of the analyzer was 1.6 mm, which corresponds to the energy resolution of about 750 meV. The experiment was performed at beamline I411 at MAX-II synchrotron radiation facility (Lund, Sweden) [26]. Undulator radiation was monochromatized using a modified Zeiss SX-700 monochromator. The samples were purchased from Sigma–Aldrich and all were used "as is" with their stated purities being ≥99% for uracil, 99% for uracil-2-^{13}C.

3. Results and discussion

Here we investigate the correlation between fragment intensities and their appearance energy (AE) values. Before going into fragment identification, an introduction to slope analysis and *ab initio* quantum chemistry calculations, which were used to aid the fragment identification, is given.

3.1. Slope analysis

All the ions formed in the sample area of the measurement equipment are accelerated by electric field to the ion detector. If all the ion fragments would have zero velocity after the fragmentation, all the ions having the same mass to charge ratio would have exactly the same flight times from the sample area to the detector. However, according to the momentum conservation law, the fragments formed in a two-body dissociation event are initially ejected toward opposite directions with velocities depending on the kinetic energy release in the process. Therefore:

1) Each ion has a flight time $T \pm \Delta T$, where T is the nominal flight time and ΔT depends on the initial velocity and a direction of the ion.
2) When plotting the coincident ion flight times in a 2D faster ion vs. slower ion flight time coordination, the coincident fragments appear as tilted patterns.

Let us now consider more complex dissociation mechanisms in the context of PEPIPICO patterns and their slope values. (The discussed mechanisms are presented in Fig. 2 and the notations of the upcoming equations follow those of Fig. 2):

1. In two-body dissociation (Fig. 2(a)) the two ions follow strict momentum anticorrelation, which is seen as a tilted pattern of PEPIPICO events with the slope value of $k = q_1/q_2$. For the two-body charge separation in molecular dication, $q_1 = q_2 = +e$ and $k = -1$. Here q is the charge of the fragment, e is the elementary charge and k is the slope value of the PEPIPICO pattern. The patterns are presented by plotting the slower ion's TOF vs. the TOF of the faster ion, and the slope is thus defined as $\Delta T_{\max}^{\text{slower}}/\Delta T_{\max}^{\text{faster}}$; the ratio of the velocity-inducied spread of the slower ion's TOF to that of the faster ion.
2. In a three-body dissociation there are three possible mechanisms: *secondary decay*, *deferred charge separation*, and *concerted dissociation*. In the last one, no general relationship between the fragmentation mechanism and the slope exist, unlike in the cases of deferred charge separation and secondary decay.
   i) In secondary decay process, Fig. 2(b), the charge separation occurs in the first step, after which the ejection of a neutral particle by one of the charged particles takes place. The observed slope depends on whether the neutral particle was ejected by the ion with the shorter or longer TOF by the lighter or heavier detected ion. The slope is thus:

$$k \approx -\frac{M_2}{M_{2a}}, \quad \text{if} \quad M_{2a} < M_1 \quad \text{and} \quad k \approx -\frac{M_{2a}}{M_1}, \quad \text{if} \quad M_{2a} > M_1.$$

   In the case of $M_{2a} = M_1$ patterns with both slopes are superimposed in the PEPIPICO map. Here it is again assumed that the energy release in the neutral fragment ejection is comparatively small.
   ii) Deferred charge separation is a two-step process with the ejection of a neutral fragment from the doubly charged ion before the charge separation as the second step as presented in Fig. 2(c). Since the kinetic energy release in the first step is usually much smaller than during the charge separation, the two fragment ions have highly correlated momenta also in

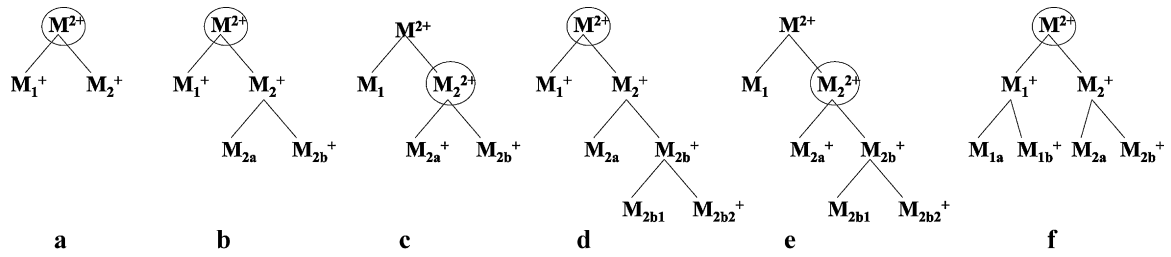

Fig. 2. Fragmentation mechanisms of doubly charged molecules. The fragment/molecule preceding the charge separation is encircled. The different *M*'s are representing the masses of the different fragments (in a.m.u).

a deferred charge separation process, producing a PEPIPICO pattern with the slope $\approx k-1$ as in the two-body case.

3. In the case of four-body dissociation there are three possible fragmentation mechanism:
   i) Fig. 2(d) is very similar to a secondary decay process, the only difference is that the secondary decay is followed by further fragmentation of the charged fragment ion. The slope for this kind process is:

$$k \approx -\frac{M_2}{M_{2b2}}, \quad \text{if} \quad M_{2b2} < M_1 \quad \text{and} \quad k \approx -\frac{M_{2b2}}{M_1}, \quad \text{if} \quad M_{2b2} > M_1.$$

   ii) Another possibility is a combination of deferred charge separation and secondary decay presented in Fig. 2(e): first a neutral fragment is ejected then charge separation takes place after which another neutral particle is ejected from one of the cations. The slope of this kind of fragmentation pattern is determined like in the case of secondary decay:

$$k \approx -\frac{M_{2b}}{M_{2b2}}, \quad \text{if} \quad M_{2b2} < M_{2a} \quad \text{and} \quad k \approx -\frac{M_{2b2}}{M_{2b}}, \quad \text{if} \quad M_{2a} > M_{2b}.$$

   iii) The third possible fragmentation mechanism is initial charge separation followed by the ejection of a neutral particle from both singly charged ions process as in Fig. 2(f). In this case the slope is determined as follows: $k \approx -\frac{M_{2b}}{M_{1b}}\frac{M_1}{M_2}$, if $M_{2b} < M_{1b}$ and $k \approx -\frac{M_{1b}}{M_{2b}}\frac{M_2}{M_1}$, if $M_{2b} > M_{1b}$.

3.2. Calculations

The purpose of the *ab initio* quantum chemistry calculations was to determine the appearance energies for various sets on final fragments, *i.e.*, the energy above the ground state of the neutral parent molecule that corresponds to the asymptotic limit of various fragmentation channels. The experimental intensities shown in Table 2 were extracted from the PEPIPICO maps by confining each pattern with a tilted rectangle and counting how many events each rectangle contains. The error bars were taken as statistic uncertainties of these numbers of events. The experimental AE values correspond to the ion fragments with optimal geometries, but the geometries of the detected ion fragments may very well be far from optimal. One might therefore disagree, whether there is any real correlation between the (AE) values presented here and the detected fragments' intensities. Nevertheless, the agreement between calculated AE values and the experimental intensities of different sets of fragments was very good for thymine [9], so similar comparison between calculations and experimental results have been carried out here also.

Computational studies were executed with the GAMESS (The General Atomic and Molecular Electronic Structure System) program [27]. The *ab initio* calculations were carried out by the unrestricted Hartree-Fock (UHF) theory [28] with the split-valence 6-311(dp) basis set [29] containing d- and p-polarization functions. The optimized structures were validated via vibrational frequencies analysis. The calculated appearance energies of fragments were estimated by subtracting the total energy of the neutral parent compound from the sum of total energies of its isolated fragments, whose optimized geometries are the lowest minima found by scanning dense grids of points in 3N-6 dimensional space (of N atoms). For instance, more than 1900 initial geometries of fragment $C_2H_3N_2O$ were optimized and they converged to 498 different equilibrium geometries. The 498 different isomers were then contrasted for retrieving the one with the lowest total energy.

3.3. Fragment identification and fragmentation processes

Identifying the fragments of multiply charged molecules from non-coincident ion time-of-flight spectra is severely hampered by the broadness of the mass peaks due to the typically high kinetic energy of the fragments. Therefore, the fragment identification and further analysis has been carried out using the two-dimensional PEPIPICO maps. Such overview maps corresponding to both samples, measured in coincidence with C 1s photoelectrons, are presented in Fig. 3 and the possible coincident fragment combinations corresponding to each pattern have been gathered in Table 1. The locations of strong patterns are labeled with mass numbers of the fragments. Experimental slope values for those patterns, that are clear enough are also presented.

It is noticeable from the PEPIPICO maps that the patterns of individual fragment pairs are generally rather blurred. This is not due to instrumental limitations (in two-body dissociation of CO_2 pattern widths of <25 ns were measured under similar settings). Instead, the reason is that in the dissociation of such relatively complex molecule, often several mechanisms contribute to the same pattern and also, as all the patterns also involve neutral fragments, the momentum correlation of the cations ranges from nonprefect to nonexistent.

A basic working assumption in our fragment identification process is that the parent molecule has only one geometry before ionization [13] and that the fragmentation can be described as a series of bond cleavage processes. Besides isotopic labeling, also the comparison with the results of thymine and 5-bromouracil, which were studied earlier [9], and slope analysis [22,30] have been carried out. The experimental slope values are determined by drawing a centerline on each pattern so that the line and the pattern are aligned as well as possible. The uncertainty of the lines are estimated to be less than 7°, which gives the error bars to the patterns in such way that the steeper the slope of a pattern, the larger the error bars. The suggested fragmentation pathways in the following text are chosen by first experimentally determining the slope of each pattern and then trying which of the processes in Fig. 2 give the best matching slope within the error limits. The discussion is given below and the identification follows the order of Table 1.

The lowest mass ion pairs correspond to (12, 28) and (13, 28) patterns on both normal and ^{13}C-uracil's maps (all masses given

Table 1
Possible cation pairs of uracil and ^{13}C-Uracil corresponding the patterns in Fig. 3(a) and (b) respectively.

Uracil Masses	Fragments		k	Masses	Fragments		k	^{13}C-Uracil Masses	Fragments		Masses	Fragments	
12, 28	C^+	$HNCH^+$ CO^+	7.1 ± 6.3	26, 43	$C_2H_2^+$ CN^+	$HNCO^+$		12, 28	C^+	$HNCH^+$ CO^+	26, 43	$C_2H_2^+$ CN^+	$N^{13}CO^+$
13, 28	CH^+ CO^+	$HNCH^+$	5.6 ± 4.1	28, 38	$HNCH^+$ CO^+	C_2N^+	1.04 ± 0.3	13, 28	CH^+ CO^+	$HNCH^+$	26, 44	$C_2H_2{}^+CN^+$	$HN^{13}CO^+$
13, 42	CH^+	NCO^+		28, 39	$HNCH^+$	C_2NH^+	0.97 ± 0.3	13, 43	CH^+	$N^{13}CO^+$	28, 38	$HNCH^+$	C_2N^+
13, 43	CH^+	$HNCO^+$			CO^+			13, 44	CH^+	$HN^{13}CO^+$		CO^+	
14, 42	CH_2^+ N^+	NCO^+		28, 40	$HNCH^+$ CO^+	$C_2NH_2{}^+C_2O^+$	1.0 ± 0.3	14, 43	CH_2^+ N^+	$N^{13}CO^+$	28, 39	$HNCH^+$ CO^+	C_2NH^+
14, 43	CH_2^+ N^+	$HNCO^+$		28, 41	$HNCH^+$ CO^+	$C_2NH_3{}^+$ C_2OH^+	0.97 ± 0.3	14, 44	CH_2^+ N^+	$HN^{13}CO^+$	28, 40	$HNCH^+$ CO^+	$C_2NH_2{}^+$ C_2O^+
16, 38	O^+	C_2N^+		28, 42	$HNCH^+$	NCO^+	1.07 ± 0.3	16, 38	O^+	$C^{13}CN^+$	28, 41	$HNCH^+$	$C_2NH_3{}^+$
16, 40	O^+	C_2NH^+ C_2O^+		28, 43	CO^+ $HNCH^+$	$HNCO^+$	2.25 ± 0.7	16, 40	O^+	$C^{13}CNH^+$ C_2NH^+ C_2O^+	28, 43	CO^+ $HNCH^+$ CO^+	C_2OH^+ $N^{13}CO^+$
27, 28	CNH^+	$HNCH^+$ CO^+		38, 43	CO^+ C_2N^+	$HNCO^+$	1.07 ± 0.3						
								27, 28	CNH^+	$HNCH^+$ CO^+	28, 44	$HNCH^+$ CO^+	$HN^{13}CO^+$
28, 28	$HNCH^+$ CO^+	CO^+		39, 4340, 43	C_2NH^+ $C_2NH_2{}^+$	$HNCO^+$ $HNCO^+$	1.04 ± 0.3 1.53 ± 0.5						
								28, 28	$HNCH^+$ CO^+	CO^+ $^{13}CNH^+$	38, 4339, 43	C_2N^+ C_2NH^+	$HNCO^+$ $HNCO^+$
28, 29	CO^+	$HNCH_2{}^+$			C_2O^+								
26, 42	$C_2H_2^+$ CN^+	NCO^+		41, 43	$C_2NH_3{}^+C_2OH^+$	$HNCO^+$	1.66 ± 0.5	28, 29	$HNCH^+$ CO^+	$^{13}CO^+$ C_2O^+	40, 44	$C_2NH_2{}^+$	$HN^{13}CO^+$
								29, 29	$^{13}CO^+$	$HNCH_2^+$	41, 44	$C_2NH_3{}^+$ C_2OH^+	$HN^{13}CO^+$

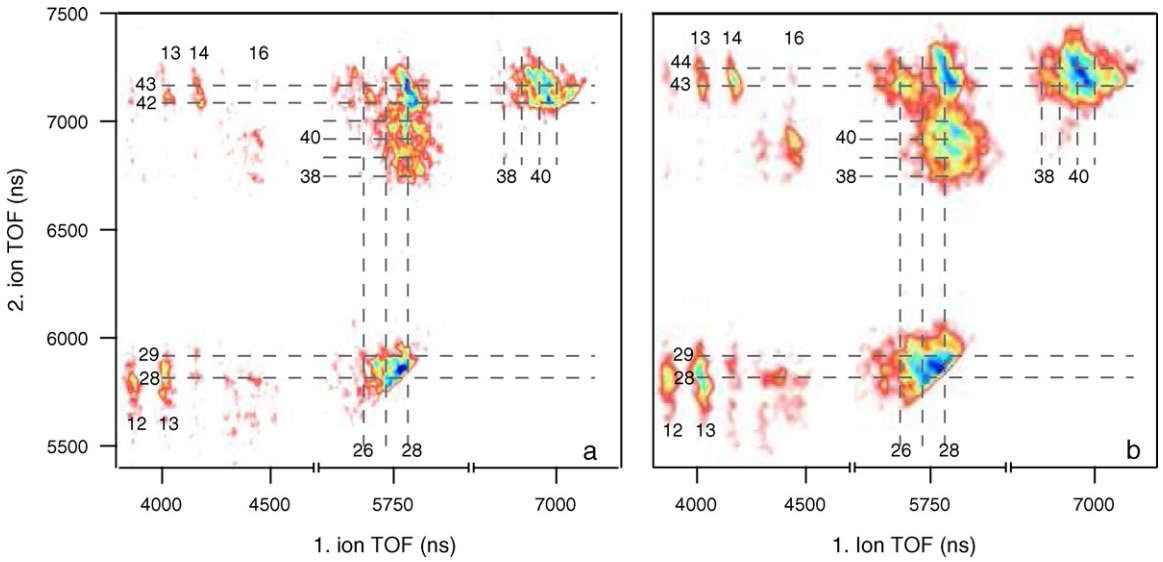

Fig. 3. Overview PEPIPICO maps of uracil (a) and ^{13}C-Uracil (b).

in a.m.u. from here on). This means that the ^{13}C is not involved in these fragments, because if the lighter fragment would contain ^{13}C, the patterns on ^{13}C-uracil's map would be (13, 28) and (14, 28). If the heavier fragment contained ^{13}C, the ^{13}C-uracil's patterns would correspond to (12, 29) and (13, 29). Because the pattens correspond to the same masses on both maps (see Fig. 3), the masses 12 and 13 must represent C^+ and CH^+ fragments, respectively, and the fragment with mass 28 is most likely $HNCH^+$. According to the simple cleavage picture, these fragments are initially located along the pyrimidine ring as in Fig. 4; at the exact same location as the corresponding pairs in thymine [9]. Fig. 4 also shows the suggested fragmentation pathways creating the detected patterns. As one can see, both above-mentioned fragment pairs have two possible formation channels. This is likely the reason why the pattern corresponding to the mass pair (13, 28) has such distorted shape, especially on ^{13}C-uracil's case in Fig. 3(b). Other possible fragments such as ^{13}C, CO^+ and $^{13}CO^+$ could also contribute to the discussed patterns, but as for example the pattern (13, 29) in Fig. 3(b) is quite weak, it is safe to assume that other fragments than C^+, CH^+ and $HNCH^+$ have much less intensity.

The next patterns in Fig. 3 correspond to masses (13, 42), (14, 42) and (16, 38/40) in case of uracil and (13, 43), (14, 43) and (16, 39/40) in case of ^{13}C-uracil. Masses 13 and 14 are CH^+ and N^+ or CH_2^+, respectively, and their coincident fragment is NCO^+ ($N^{13}CO^+$ in case of ^{13}C-uracil). Because the patterns on ^{13}C-uracil's map (Fig. 3(b)) are shifted one mass unit up compared to those in normal uracil's map (Fig. 3(a)) it is very clear that the heavier fragment contains now the C2 carbon. There are also weak patterns corresponding to masses 43 on uracil's map and 44 on ^{13}C-uracil's map, which indicates that the NCO^+ ($^{13}NCO^+$) patterns result from further fragmentation of $HNCO^+$ ($H^{13}NCO^+$), which is the fragment corresponding to mass 43 (44). It is perhaps unexpected that $HNCO^+$ fragments further to NCO^+ because neither thymine nor 5-bromouracil exhibited such behavior [9]. The pattern (16, 38) although being very weak and therefore conclusions about it are highly suspect, is also quite interesting, because it has shifted to (16, 39) in ^{13}C-uracil's map. This means that the heavier fragment must be C_2N^+ ($^{13}CCN^+$) the lighter fragment being O^+, again the heavier fragment contains the C2 carbon. One notices that the initial site of fragments where the corresponding ^{13}C-uracil's fragment contains ^{13}C, is very well determined. The pattern (16, 40) has two possible

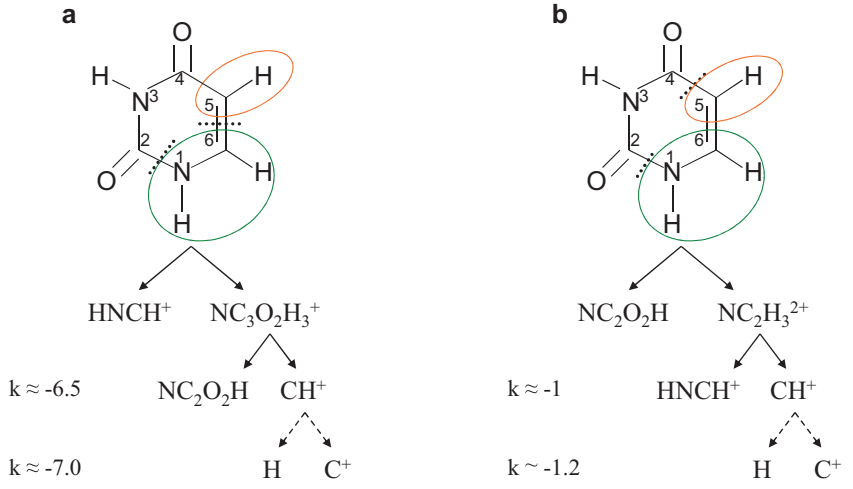

Fig. 4. Fragmentation channels for uracil's coincident fragments with masses (12, 28) and (13, 28). The *k* values are theoretical values calculated using the equations determined previously in this section. The process(es) (a) corresponds to processes (b) or (d) of Fig. 2 and the process(es) (b) corresponds to processes (c) or (e) of Fig. 2.

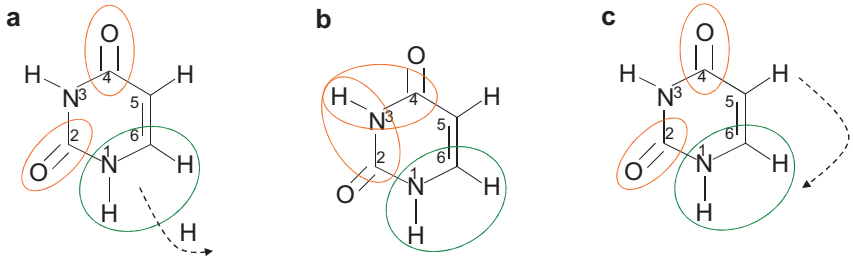

Fig. 5. Sites of origins of coincident fragments corresponding to patterns with masses (27, 28) (a), (28, 28) (b) and (28, 29) (c) in Fig. 3 (a).

assignments resented in Table 1, it is clear that the C2 carbon is not included, because if it was, there would be a pattern corresponding to (16, 39) on uracil's map (Fig. 3(a)) and there is not.

Next patterns on Table 1 are (27, 28), (28, 28) and (28, 29) for uracil and (27,28), (28,28), (28,29) and (29,29) for ^{13}C-uracil. These patterns are strong, but quite blurry, so no detailed fragmentation pathways are given here or in Fig. 5, only the fragments and sites of origins. We discuss here only about those fragments believed to be the most common although all the fragments presented in Table 1 probably contribute. Starting with pattern (27, 28); proposed fragments are HNC^+ and CO^+ as in Fig. 5(a). This is justified, since in case of ^{13}C-uracil, the proposed fragments would create not only the (27, 28) pattern, but also a pattern corresponding to (27, 29). Closer investigation of the ^{13}C-uracil's map (Fig. 3(b)) indicates that indeed also a pattern corresponding to (27, 29) exists. Another possible fragment assignment for (27, 28) is (CNH^+, $HCNH^+$), which in case of ^{13}C-uracil would spread, because of the ^{13}C, into two pattens; (27, 28) and (28, 28) (see Fig. 5(b)) which are present in Fig. 3(b). Pattern (28, 28) is clearly the most intensive on both samples' maps. This means, that although both CO moieties presented in Fig. 5(a) are possible to appear in coincidence with $HNCH^+$, the fragment pair corresponding to (28, 28) is most likely ($HNCH^+$, CO^+) where the CO^+ fragment contains particularly the C4 carbon. Only then ($HNCH^+$, CO^+) is the only pair corresponding to masses (28, 28) in case of uracil and ^{13}C-uracil. Lastly, perhaps the most interesting pattern; (28, 29) on uracil's map (Fig. 3(a)). The mass 29 indicates that a hydrogen migration takes place during the dissociation process, which is very unique. Because ^{13}C-uracil creates a pattern (29, 29), but not patterns (28, 30) or (29, 30), the hydrogen must migrate into HNCH moiety. This is because both CO parts of the molecule are in equal positions from the hydrogens' points of view and if a hydrogen was to migrate into another CO parts of the molecule, there is no reason, why this would not happen with the other CO part too. Therefore the (28, 29) pattern of uracil corresponds most likely to (CO^+, $HNCH_2{}^+$), as presented in Fig. 5(c).

Like some of the previous pairs, also those corresponding to masses (26, 42) and (26, 43) in the case of uracil do not have corresponding pairs from the same pyrimidine ring fractions in the case of thymine and 5-bromouracil [9]. The corresponding fragments in case of ^{13}C-uracil, are (26, 43) and (26, 44), which means that the heavy fragments are NCO^+ and $HNCO^+$ ($^{13}NCO^+$ and $H^{13}NCO^+$ for ^{13}C-uracil). Table 1 suggests two light fragments, but as there is no pattern corresponding to (27, 42/43), it is unlikely that the $HNCH^+$ would only fragment further into CN^+ and not into CNH^+. Therefore authors believe the the fragment with mass 26 is $C_2H_2{}^+$.

The next set of patterns is a bit blurred since the patterns are long and relatively weak. On both maps of Fig. 3, the patterns correspond to mass 28 on the *x*-axis and masses 38–41 on the *y*-axis. The possible fragment combinations are presented in Table 1 and the suggested fragmentation pathways are those in Fig. 6. The channel in Fig. 6(a) spans over all four patterns considered here whereas the process in Fig. 6(b) covers only the two heaviest ones. It is likely that both processes do occur, but the process (b) is more probable – supported by the fact that thymine produces corresponding fragments for those of process (b) but not for those of process (a) [9].

The most intense pattern of all is the one corresponding masses (28, 43) for uracil and (28, 44) for ^{13}C-uracil, which means that the heavy pattern is again $HNCO^+$ ($H^{13}NCO^+$ for ^{13}C-uracil). Although Table 1 gives two possibilities for the fragment with mass 28, we expect that the pattern consist mostly of $HNCH^+$. This is because according to our calculations, the ($HNCH^+$, $HNCO^+$) pair has much lower appearance energy than (CO^+, $HNCO^+$) and because thymine and 5-bromouracil also had a strong fragmentation channel for ($HNCH^+$, $HNCO^+$) [9]. What thymine or 5-bromouracil did not exhibit, is the further fragmentation of the $HNCO^+$ fragment, which seems to be quite common for uracil (see patterns (28, 42) and (28, 43) on Fig. 3(a) and (b) respectively). It is perhaps a little misleading to say that in some cases the $HNCO^+$ fragment dissociates further, because the coincident pairs ($HNCH^+$, $HNCO^+$) and ($HNCH^+$, NCO^+) have very different fragmentation pathways as one can see from Fig. 7.

The last four patterns discussed here are located differently on uracil's map than on ^{13}C-uracil's map (see Fig. 3). In the case of uracil, all patterns are on same row, but on ^{13}C-uracil's map there are two rows. This means that there are probably two processes as described in Fig. 8 that produce the detected patterns. Because ^{13}C-uracil seems not to produce $C_2NH_n{}^+$ fragments where $n = 0,1$ in coincidence with $HN^{13}CO^+$ it would be quite unexpected, if it would do so with $HN^{13}CO^+$. Therefore, the authors propose the process (a) in Fig. 8 for patterns (38, 43), (39, 43) and (40, 43) (both samples) and process (b) in Fig. 8 for patterns (40, 43) and (41, 43) ((40, 44) and (41, 44) for ^{13}C-uracil). We do not totally exclude $C_2NH_n{}^+$ fragments (where $n = 2,3$) and in fact, our calculations, which are described in the next section, suggest that $C_2NH_{2,3}{}^+$ are much more likely to appear in coincidence with $HNCO^+$ than $C_2OH_{0,1}{}^+$. It is just not very logical, which is the reason for preferring the process (b) of Fig. 8.

3.4. Pattern intensities and appearance energies

Next we study the correspondence between the calculated AE values and experimental intensities of the different fragments. The values are presented in Table 2 and the intensities vs. the calculated AE values are also plotted in Fig. 9 that also shows similar data for thymine, as a reference.

As one can see, uracil (as well as thymine) has a rising trend of the AE as a function of decreasing intensity. This trend is quite scattered and with several fragments, the correlation between AE values and the intensities of the detected fragments is weak. For some fragments, an explanation for large deviations from the trend could be as follows: for example, the (41, 43)-pattern most likely results from the process:

$$U^{2+} \rightarrow HNCO^+ + C_3H_3NO^+ \rightarrow HNCO^+ + C_2H_3N^+ + CO, k \approx -1.7.$$

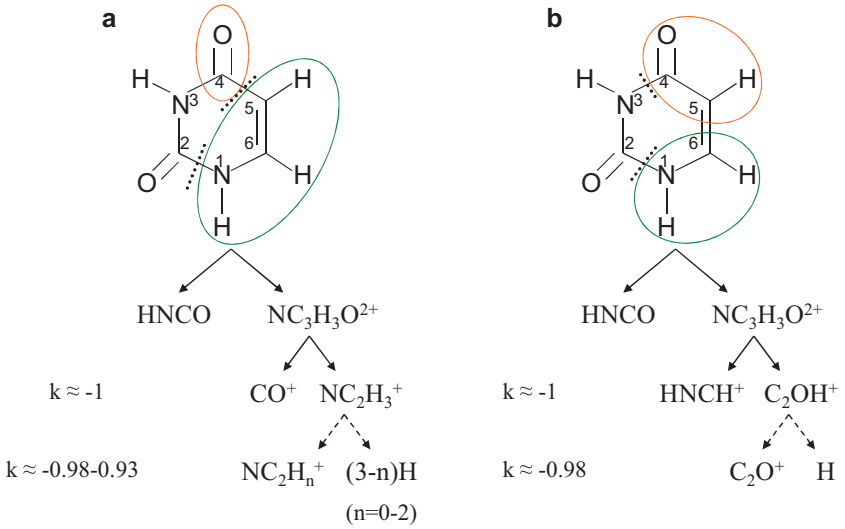

Fig. 6. Fragmentation channels for uracil's coincident fragments with masses (28, 38–41). The *k* values are theoretical values calculated using the equations determined previously in this section. Processes in both (a) and (b) correspond to processes (c) or (e) of Fig. 2.

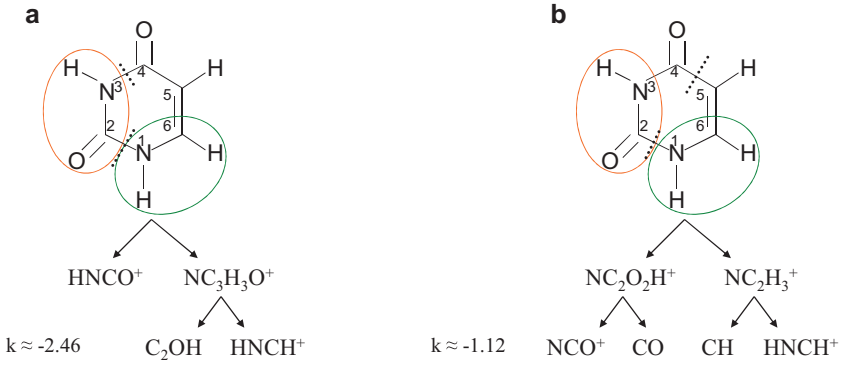

Fig. 7. Fragmentation channels for uracil's coincident fragments with masses (28, 43) and (28, 42). The *k* values are theoretical values calculated using the equations determined previously in this section. The processes (a) and (b) correspond to processes (c) and (f) of Fig. 2 respectively.

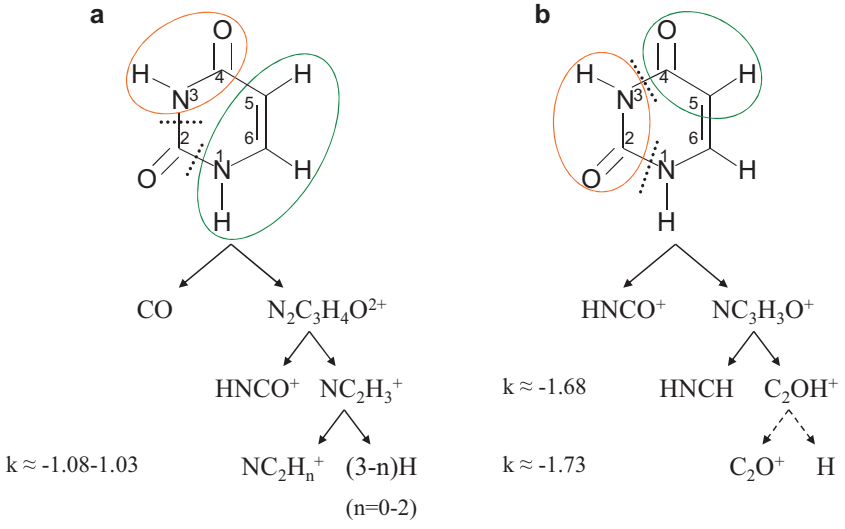

Fig. 8. Fragmentation channels for uracil's coincident fragments with masses (38–41, 43). The *k* values are theoretical values calculated using the equations determined previously in this section. The process (a) corresponds to processes (e) of Fig. 2 and the process(es) (b) corresponds to processes (b) or (d) of Fig. 2.

Table 2
Cation pairs of uracil patterns in Fig. 3(a) with their experimental intensities and calculated AE values. Those processes believed to be less likely are presented in brackets.

M_1, M_2	I_{exp} (relative)	Cation1	Cation2	Neutral fragment(s)	AE (eV)
12, 28	0.26 ± 0.1	C^+	$HNCH^+$	$C_2HN_2O + H$	28.0
13, 28	0.35 ± 0.1	CH^+	$HNCH^+$	C_2HN_2O	25.0
27, 28	0.81 ± 0.07	CNH^+	CO^+	HNCO + CH + H	29.2
		(CNH^+	$HNCH^+$	$C_2HO + O$)	29.9
28, 28	1.00 ± 0.08	$HNCH^+$	CO^+	C_2H_2NO	23.9
		($HNCH^+$	CO^+	CH + HNCO)	27.5
28, 29	0.46 ± 0.08	CO^+	$HNCH_2^+$	C_2HNO	24.4
28, 38	0.45 ± 0.08	CO^+	C_2N^+	$HNCO + H_2 + H$	34.3
28, 39	0.60 ± 0.08	CO^+	C_2NH^+	$HNCO + H_2$	31.0
28, 40	0.62 ± 0.08	$HNCH^+$	C_2O^+	HNCO + H	25.9
		(CO^+	$C_2NH_2^+$	HNCO + H)	26.5
28, 41	0.72 ± 0.07	$HNCH^+$	C_2OH^+	HNCO	21.6
		(CO^+	$C_2NH_3^+$	HNCO)	22.6
28, 42	0.45 ± 0.08	$HNCH^+$	NCO^+	$C_2HO + H$	29.0
28, 43	0.96 ± 0.06	$HNCH^+$	$HNCO^+$	C_2HO	22.5
38, 43	0.31 ± 0.1	C_2N^+	$HNCO^+$	$CO + H_2 + H$	27.8
39, 43	0.56 ± 0.08	C_2NH^+	$HNCO^+$	$CO + H_2$	28.2
40, 43	0.87 ± 0.06	C_2O^+	$HNCO^+$	HNCH + H	28.7
		($C_2NH_2^+$	$HNCO^+$	CO + H)	23.6
41, 43	0.68 ± 0.07	C_2OH^+	$HNCO^+$	HNCH	24.4
		($C_2NH_3^+$	$HNCO^+$	CO)	19.8

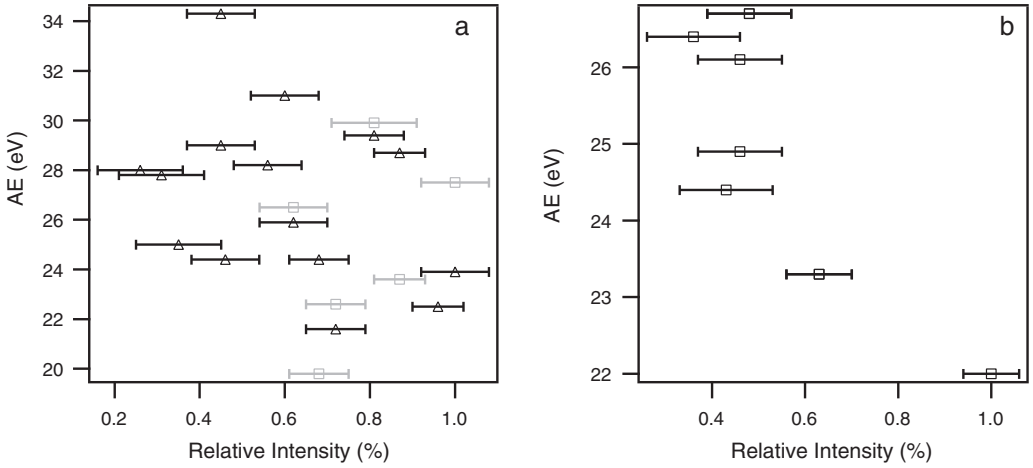

Fig. 9. Relative intensities (with error bars) vs. calculated AE values of different fragmentation channels of uracil (a) and thymine (b). The gray markers belong to the processes presented in brackets in Table 2.

If the $C_2NH_3^+$ fragments further:

$$U^{2+} \rightarrow HNCO^+ + C_3H_3NO^+ \rightarrow HNCO^+ + C_2H_3N^+ + CO \rightarrow HNCO^+ + HNCH^+ + CO + CH, k \approx -2.48.$$

This process is very similar to that in Fig. 7(a). In fact, it is impossible to say if it is the process (a) in Fig. 7 or the process presented above that produces the (28, 43) pattern, as both processes give the exact same slope. The lack of intensity in pattern (41, 43) can be explained by the instability of the $C_3H_3NO^+$-fragment. The trend in thymine (Fig. 9(b)) is largely defined by a single dominant fragmentation channel that has also the lowest AE. In uracil, however, there is no such single dominant process. The reason is probably the lack of the methyl group in uracil. The methyl group seems to alter the dissociation process just enough so that the ($HNCH^+$, $HNCO^+$) fragment becomes clearly the most abundant ion pair to result from the core ionization.

4. Conclusions

The present study confirms that the fragmentation of uracil following the C 1s core ionization can very well be described as a series of bond cleavages, starting from breaking up the pyrimidine ring and followed by one or multiple steps of secondary fragment dissociations. It has become clear that the pyrimidine ring itself, being a very stable form, does not undergo any geometrical rearrangements preceding the separation of the fragments; only the fraction of the ring initiates the restructuring process(es) of the ring fragment(s) towards energetically more favorable form.

The ionic fragments following the core ionization of uracil molecule are quite similar to those from core ionization of thymine and 5-bromouracil. For example the ($HNCO^+$, $HNCH^+$) pair is one of the most common pairs for all three samples. Also fragments CH_n^+, (n = 0,1) CO^+, $C_2NH_n^+$, (n = 0–3) and C_2OH^+ have corresponding fragments in case of thymine and/or 5-bromouracil. The above mentioned fragments are also strongly present in the fragmentation of singly ionized uracil [10,11]. This result supports the conclusion that no matter what functional groups are attached to a pyrimidine ring, the fragmentation mainly follows a certain pattern where the ring "prefers" the fracture of certain bonds.

Some new features appear in uracil, not observed in thymine or 5-bromouracil. First is the detection of the C_2N^+ fragment containing C2 carbon. Second is the detection of $HNCO^+$ fragment containing the C4 carbon. This is quite unexpected, since with thymine or 5-bromouracil we assumed that the carbon in $HNCO^+$

would always be the C2 carbon. Now we know that it not so and also have a more clear picture of the fragmentation of pyrimidine derivatives in general: it is very likely that the carbon atom in $HNCO^+$ fragment is no other than C2, but it is clear too that such fragmentation channel(s) which produce $HNCO^+$ containing different carbon atom than C2 also exist. The third observation is more a difference than a unique feature; the intensity difference between the fragments is smaller in the case of uracil than with thymine or 5-bromouracil and also less very weak patterns exist on uracil's PEPIPICO map. These effects are probably due to the replacement of the hydrogen atom with a methyl group (or a bromine atom), but in order to get more insight to these effects more studies with pyrimidine derivatives or pyrimidine itself would be beneficial.

Acknowledgements

Financial support from the Academy of Finland, the EU Transnational Access to Research Infrastructures programme and from the Graduate School of Materials Research of the Ministry of Education of Finland is acknowledged. E.N. and U.J. want to thank the Estonian Ministry of Education and Research (target financed theme SF0180046s07) for financial support, also NordForsk are gratefully acknowledged. The authors thank the staff of MAX-lab for their help during the experiments and express their gratitude to the Electron Spectroscopy Group of the University of Oulu for the opportunity to share their experimental equipment. The research leading to these results has received funding from the European Community's Seventh Framework Programme (FP7/2007-2013) under grant agreement no. 226716.

References

[1] G.F. Joyce, Nature 418 (2002) 214.
[2] E.A. Kuzicheva, M.B. Simakov, Adv. Space Res. 23 (2) (1999) 391.
[3] M.B. Simakov, E.A. Kuzicheva, A.E. Antropov, N. Ya Dodonova, Adv. Space Res. 30 (6) (2002) 1489.
[4] A. Shimoyama, S. Hagishita, K. Harada, Geochem. J. 24 (1990) 343.
[5] I.W.M. Smith, D. Talbi, E. Herbst, Astron. Astrophys. 369 (2001) 611.
[6] V.A. Basiuk, J. Douda, Planet. Space Sci. 47 (1990) 577.
[7] Z. Martins, O. Botta, M.L. Fogel, M.A. Sephton, D.P. Glavin, J.S. Watson, J.P. Dworkin, A.W. Schwartz, P. Ehrenfreund, Earth Planet. Sci. Lett. 270 (2008) 130.
[8] M. Nuevo, S.N. Milam, S.A. Sandford, J.E. Elsila, J.P. Dworkin, Astrobiology 9 (7) (2009) 683.
[9] E. Itälä, D.T. Ha, K. Kooser, E. Rachlew, M.A. Huels, E. Kukk, J. Chem. Phys. 133 (2010) 154316.
[10] H.-W. Jochims, M. Schwell, H. Baumgärtel, S. Leach, Chem. Phys. 314 (2005) 263.
[11] M. Imhoff, Z. Deng, M.A. Huels, Int. J. Mass Spectrom. 262 (2007) 154.
[12] S. Denifl, B. Sonnweber, G. Hanel, P. Scheier, T.D. Märk, Int. J. Mass Spectrom. 238 (2004) 47.
[13] V. Feyer, O. Plekan, R. Richter, M. Coreno, G. Vall-llosera, K.C. Prince, A.B. Trofimov, I.L. Zaytseva, T.E. Moskovskaya, E.V. Gromov, J. Schirmer, J. Phys. Chem. A 113 (2009) 5736.
[14] A. Haug, S. Schweizer, F. Latteyer, M. Benedetta, H. Peisert, C. Ochsenfeld, T. Chass, ChemPhysChem 9 (2008) 740.
[15] J. Peeling, F.E. Hruska, D.M. McKinnon, M.S. Chauhan, N.S. McIntyre, Can. J. Chem. 56 (1978) 2405.
[16] T. Schlathölter, F. Alvarado, R. Hoekstra, Nucl. Instrum. Methods Phys. Res. B 233 (2005) 62.
[17] S. Leach, J. Electron Spectrosc. Relat. Phenom. 41 (1986) 427.
[18] P.J. Richardson, J.H.D. Eland, P. Lablanquie, Org. Mass Spectrom. 21 (1986) 289.
[19] R.D. Molloy, J.H.D. Eland, Chem. Phys. Lett. 421 (31) (2006).
[20] C.J. Danby, J.H.D. Eland, Int. J. Mass Spectrom. Ion Phys. 8 (1972) 153.
[21] M. Simon, T. LeBrun, P. Morin, M. Lavollée, J.L. Maréchal, Nucl. Instrum. Methods B 62 (1991) 167.
[22] J.H.D. Eland, Laser Chem. 11 (1991) 259.
[23] C. Harada, S. Tada, K. Yamamoto, Y. Senba, H. Yoshida, A. Hiraya, S. Wada, K. Tanaka, K. Tabayashi, Radiat. Phys. Chem. 75 (2006) 2085.
[24] E. Kukk, R. Sankari, M. Huttula, A. Sankari, H. Aksela, S. Aksela, J. Electron Spectrosc. Relat. Phenom. 155 (2007) 141.
[25] M. Huttula, S. Heinäsmäki, H. Aksela, E. Kukk, S. Aksela, J. Electron Spectrosc. Relat. Phenom. 156–158 (2007) 270.
[26] M. Bässler, A. Ausmees, M. Jurvansuu, R. Feifel, J.-O. Forsell, P. de Tarso Fonseca, A. Kivimäki, S. Sundin, S.L. Sorensen, R. Nyholm, O. Björneholm, S. Aksela, S. Svensson, Nucl. Instrum. Methods Phys. A 469 (2001) 382.
[27] M.W. Schmidt, K.K. Baldridge, J.A. Boatz, S.T. Elbert, M.S. Gordon, J.J. Jensen, S. Koseki, N. Matsunaga, K.A. Nguyen, S. Su, T.L. Windus, M. Dupuis, J.A. Montgomery, J. Comput. Chem. 14 (1993) 1347, GAMESS http://www.msg.chem.iastate.edu/gamess/.
[28] J.A. Pople, R.K. Nesbet, J. Chem. Phys. 22 (1954) 571.
[29] R. Krishnan, J.S. Binkley, R. Seeger, J.A. Pople, J. Chem. Phys. 72 (1980) 650.
[30] E. Itälä, E. Kukk, D.T. Ha, S. Granroth, A. Caló, L. Partanen, H. Aksela, S. Aksela, J. Chem. Phys. 131 (2009) 114314.